Chapter 3
Structural Peculiarities and Properties of Silver-Containing Polymer Nanocomposites

V. Demchenko, S. Riabov, S. Kobylinskyi, L. Goncharenko, and N. Rybalchenko

3.1 Introduction

During the last decades, the interest in studying of nanosize particles of different metals and their oxides has constantly grown up [1–4]. Primarily, it is due to their unique characteristics, dramatically different from their analogues – micro-scale size objects. So, this fact opens new possibilities for diverse applications of nanomaterials, having advanced properties in industrial areas.

Hybrid materials, containing silver nanoparticles, show promising features for the design of catalytic systems, and they are currently used in optoelectronics and nanophotonics [5–10]. In turn, nanocomposite materials [10–12] with silver nanoparticles have found a wide application as effective antibacterial and antiviral preparations. Within the recent years (due to the emergence of microorganisms resistant to known antimicrobial agents), demand in new high-effective substances for saturation of dressing materials in medical facilities, as well as for the formation of antimicrobial coatings for providing of sterile conditions in biological and medical laboratories, for food packaging, for design of antimicrobial air filters for hospitals' and microbiological laboratories ventilation, etc., has appeared and is rapidly growing. Metal nanoparticles, such as copper, silver, and zinc, are in the focus of the researchers involved into development of effective antimicrobial agents due to their biocidal activity and high stability in extremal conditions.

V. Demchenko (✉) · S. Riabov · S. Kobylinskyi · L. Goncharenko
Institute of Macromolecular Chemistry, The National Academy of Sciences of Ukraine, Kyiv, Ukraine

N. Rybalchenko
Zabolotny Institute of Microbiology and Virology, The National Academy of Sciences of Ukraine, Kyiv, Ukraine

O. Fesenko, L. Yatsenko (eds.), *Nanochemistry, Biotechnology, Nanomaterials, and Their Applications*, Springer Proceedings in Physics 214,
https://doi.org/10.1007/978-3-319-92567-7_3

Developing of such materials is not possible without fundamental researches and studying their structure and physicochemical and mechanical properties.

The current review of scientific sources revealed that data concerning investigations of structural organization and physical, mechanical, and antimicrobial properties of Ag-containing nanocomposites obtained by chemical or thermal reduction of Ag^+ ions in the interpolyelectrolyte–metal complexes are not published yet.

So, the aim of this work is to study the structural organization and thermomechanical and antimicrobial properties of nanocomposites prepared involving natural and synthetic polymers – pectin, polyethyleneimine, poly(4-vinylpyridine), and Ag nanoparticles – obtained by the chemical and thermal reduction of silver ions in the interpolyelectrolyte–metal complexes.

3.2 Structural Formation and Thermomechanical Properties of Polymer Nanocomposites Based on Pectin–Poly(4-Vinylpyridine) Interpolyelectrolyte Complexes and Ag Nanoparticles

To obtain the interpolyelectrolyte complexes (IPEC), pectin–poly(4-vinylpyridine) (P4VP); the interpolyelectrolyte–metal complexes (IMC), pectin–Ag^+–P4VP; and nanocomposites of IPEC–Ag, the following reagents were used: pectin sodium salt (Na-pectin), obtained by mixing citrus pectin production ("Cargill Deutschland GmbH" (Germany)), $M = 3{\cdot}10^4$, with NaOH; hydrochloride poly(4-vinylpyridine) (P4VP-Cl), obtained by protonation of pyridine ring poly(4-vinylpyridine) (Aldrich), $M_w = 6{\cdot}10^4$, with HCl; silver (I) nitrate ($AgNO_3$) (Aldrich) with $M = 169.9$; and sodium borohydride ($NaBH_4$) (Aldrich) with $M = 37.83$.

IPEC samples were formed via mixing of 5% aqueous solutions of Na-pectin and P4VP-Cl taken at an equimolar ratio, at $T = 20 \pm 2$ °C.

$$—COO^-Na^+ + Cl^-H^+N— \rightarrow —COO^-H^+N + Na^+Cl^-$$

While mixing of anion and cation polyelectrolytes' (PE) water solutions, one could observe immediate formation of clots as a result of a process of molecular "recognition" and self-assembly of oppositely charged PE macromolecules [13]. These clots, which are IPEC, were formed as thin films on polytetrafluorethylene plates, dried at $T = 20 \pm 2$ °C to a constant mass, then washed in distilled water getting reached neutral pH, and then dried again till to a constant mass. The resulting films were 100–500 μm thick.

IMC samples were prepared via immersion of IPEC films into an aqueous solution of $AgNO_3$ with a concentration of 0.1 mol/L at $T = 20 \pm 2$ °C for 24 h. The colorless IPEC films became dark red.

The absorption capacities of films, A (mmol/g), were calculated through the formula [14]:

$$A = \left(c_{in} – c_{eq}\right) V/m,$$

where m is the mass of the absorbent, V is the volume of the solution, and c_{in} and c_{eq} are the initial and the equilibrium concentrations of silver ions. For IMC films $A = 2.2$ mmol/g.

The chemical reduction of Ag^+ ions in the IMC was realized with $NaBH_4$ (a molar ratio of $[BH_4^-]:[Ag^+] \geq 1.0$) in an alkaline medium (pH 10.8) in a solvent mixture of water–isopropanol (4:1 vol %) at $T = 20 \pm 2$ °C for 3 h (until the release of gaseous bubbles ceased). The concentration of $NaBH_4$ in the aqueous alcohol solution was 0.1 mol/L. As a result of the reduction, IMC films changed color from red to a metallic silver one.

The features of the structuring of the IPEC (pectin–P4VP), the IMC (pectin–Ag^+–P4VP), and nanocomposites of IPEC–Ag were studied by wide-angle X-ray scattering (WAXS) with a DRON-4-07 diffractometer (scientific-production company "Burevestnik," Russia), whose X-ray optical scheme was used to "pass" primary-beam radiation through samples.

The heterogeneous structuring of these polymeric systems (at the nanometer level) was studied via small-angle X-ray scattering (SAXS) with a CRM-1 camera (Orel scientific equipment factory, Russia), having a slit collimator of the primary irradiation beam made via the Kratky method. The geometric parameters of the camera satisfied the condition of infinite height of the primary beam [15]. The intensity profiles were normalized to the volume of X-ray scattering and the attenuation factor of the primary beam of the test sample.

All X-ray diffraction studies were performed at $T = 20 \pm 2$ °C in CuK_α radiation monochromated with a Ni filter.

Thermomechanical studies of polymer systems were conducted using the penetration method in the mode of a uniaxial constant load ($\sigma = 0.5$ MPa) with a UIP-70 M device (central design engineering bureau of the special instrument making of the Russian Academy of Sciences). Linear heating of samples was performed at a rate of 2.5 °C/min in the temperature range 0 to +250 °C. Relative penetration (%) was calculated as:

$$\varepsilon = (\Delta l / l_0) \cdot 100,$$

where Δl is penetration (μm) at certain temperature and l_0 is the initial thickness of the sample (μm).

Comparing of the WAXS diffractograms of the cationic and anionic polyelectrolytes on whose basis the IPEC was formed (see Fig. 3.1), it was found that P4VP has only short-range ordering while translated in bulk fragments of the main macromolecular chains and their lateral branches – pyridine ring (curve *1*) – and pectin has an amorphous–crystalline structure (curves *4*).

The analysis of the atomic structure of macromolecules P4VP showed that low-intensity peak at $2\theta_{max} \sim 10{,}6^\circ$ describes the near arrangement of basic macromolecular chains, while $2\theta_{max} \sim 19{,}7^\circ$ characterizes pyridine ring (Fig. 3.1, curve *1*).

Herewith, the average value of d period of the short-range ordering of fragments of basic macrochains at their positioning in a space (in a volume of P4VP) according

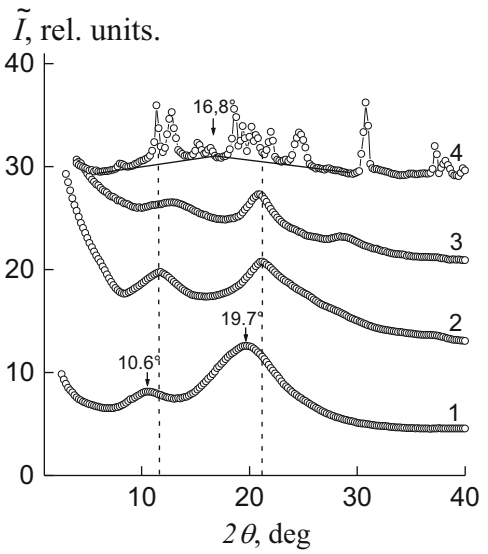

Fig. 3.1 Wide-angle X-ray diffractograms of (*1*) the P4VP, (*2*) the IPEC pectin–P4VP, (*3*) a pectin film, and (*4*) a pectin powder

to the Bragg equation is:

$$d = \lambda(2\sin\theta_m)^{-1},$$

where λ is the wavelength of the characteristic X-ray radiation, which is 8.3 Å, whereas Bragg in space at rotation cycles pyridine – 4.5 Å (λ = 1.54 Å for CuK_α radiation).

On the X-ray profile of pectin, whose sample is a powder (Fig. 3.1, curve *4*), there are many singlet and multiplet diffraction maxima having an imaginary amorphous halo with a vertex at $2\theta_m \sim 16.8°$ in the background, indicating to the amorphous–crystalline structure of this polysaccharide.

The relative crystallinity of pectin, X_{cr}, was determined via the Mathews method [16]:

$$X_{cr} = Q_{cr}(Q_{cr} + Q_{am})^{-1} \cdot 100,$$

where Q_{cr} is the area of the diffraction maxima, characterizing the crystalline structure of the polymer and $Q_{cr} + Q_{am}$ is the total area of the X-ray pattern in the range of scattering angles $2\theta_1 \div 2\theta_2$, where the amorphous–crystalline structure of the polymer manifests itself. The calculations showed that X_{cr} approximates the value of 65%.

In turn, effective crystallite size L of pectin determined via the Scherrer method [17]:

$$L = K\lambda(\beta\cos\theta_m)^{-1},$$

where K is a constant related to a shape of the crystallites ($K = 0.9$ if their shape is unknown) and β is the angular half-width (width at a half-height) of the singlet of a discrete diffraction maximum, showed that the average L value is 17.5 nm (for the calculation, singlet diffraction maxima at $2\theta_m = 18.7°$ and 30.8° were applied).

However, the X-ray pattern of the pectin sample in the form of a film prepared from a 5% aqueous solution displays only contours of the groups of diffraction maxima with basic intensities that are present on the X-ray pattern of the pectin powder (Fig. 3.1, curves *3*, *4*). This circumstance indicates a low rate of pectin crystallization, as well as the relaxation character of the structurization processes in the polymers.

IPEC formed from pectin and P4VP is characterized by short-range ordering during translation of fragments of oppositely charged polyelectrolyte macromolecular chains in a space. This fact is confirmed by the appearance of diffuse diffraction maximum at $2\theta_m \sim 21.2°$ on the X-ray profile of the IPEC sample (see Fig. 3.1, curve *2*). The average value for the period of short-range ordering of macromolecular chains' fragments of oppositely charged polyelectrolytes in the IPEC (the average Bragg distance between chains of the polyanion and the polycation) is equal to 4.2 Å.

The following fact should be taken into consideration: in the IPEC profile obtained for equimolar quantity of pectin and P4VP, the angular location of the secondary (rated by intensity) diffraction maximum is shifted from 10.6° to 11.8° comparing with P4VP (Fig. 3.1, curves *1, 2*), while the average Bragg distance (d) between P4VP's main macrochains (as part of IPEC) is falling down from 8.3 Å to 7.5 Å.

Once the pectin–Ag^+–P4VP IMC is formed, the diffraction pattern changes. This is confirmed by the appearance of a low-intense diffuse diffraction maximum at $2\theta_m \sim 11.0°$ (Fig. 3.2, curve *2*) in the presence of a low-intensity amorphous halo, which, unlike that for the IPEC, has an angular position at $2\theta_m \sim 21.4°$. According to [18], this diffraction maximum characterizes the existence of interpolyelectrolyte–metal complexes between the ions (Ag^+) and ligands. Taking into account the angular position of this diffraction peak on the X-ray diffractogram of the IMC, average Bragg distance d between the macromolecular chains of polyelectrolytes coordinated with Ag^+ ions is found to be 8.0 Å.

Chemical reduction of the Ag^+ ions in the IMC by sodium borohydride results in formation of a nanocomposite based on the IPEC and Ag. In the nanocomposite's profile (Fig. 3.2, curve *3*), one can see that the low-intense diffraction maximum at $2\theta_m \sim 11.0°$, which is typical of the above interpolyelectrolyte–metal complexes, is absent, unlike two intensity diffraction peaks appeared at $2\theta_m \sim 37.8°$ and 43.6°, corresponding to the crystallographic plan of the face-centered cubic lattice of silver with (111) and (200) indexes, respectively, thus confirming presence of metallic silver in the polymeric system. Moreover, diffraction maximum intensity at $2\theta_m \approx 20.8°$, characterizing structure of IPEC "pectin–P4VP," is enhanced.

Effective size L of Ag nanoparticle crystallites in the IPEC proved to be 4.0 nm (for the calculation, diffraction maxima at $2\theta_m = 37.8°$ and 43.6° were used, curve *3*).

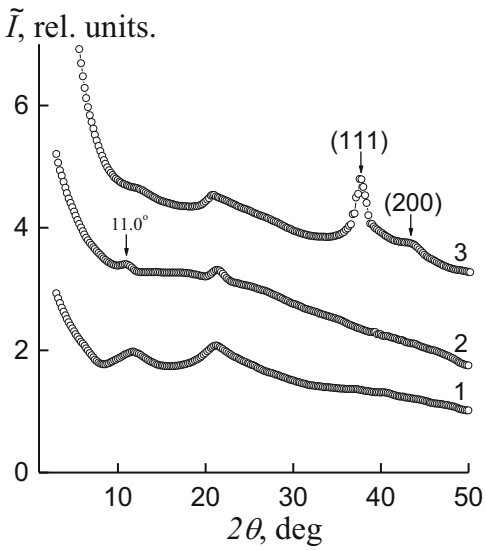

Fig. 3.2 Wide-angle X-ray diffractograms of (*1*) the IPEC pectin–P4VP, (*2*) the IMC pectin–Ag^+–P4VP, and (*3*) the IPEC–Ag nanocomposite

The revealed peculiarities and changes in structures while transiting from the IPEC to IMC and IPEC–Ag nanocomposites form the basis for the further study of their structural heterogeneity.

Analyzing the profiles of small-angle X-ray scattering of the polymer systems, presented in [19, 20], as dependences of $\tilde{I}$ on q (Fig. 3.3) and $s^3\tilde{I}$ on s^3, where $\tilde{I}$ is the intensity of scattering without the collimation correction and $q = (4\pi/\lambda)\sin\theta = 2\pi s$, all these systems have heterogeneous structure, i.e., contrast electron densities $\Delta\rho$ ($\Delta\rho = \rho - <\rho>$, where ρ and $<\rho>$ are the local and average values of the electron density, respectively) are present in their volumes. This result means that in the IPEC, IMC, and the nanocomposites based on the IPEC and Ag, there are at least two types of regions of heterogeneity with different values of local electron density ρ.

As one can see, scattering intensity and thus $\Delta\rho$ value are increasing for these systems in the following rank: IPEC pectin P4VP → IMC pectin–Ag^+–P4VP → nanocomposite IPEC–Ag (Fig. 3.3, curves *1–3*). However, the absence of the interference peak in the all profiles indicates the stochastic nature of the location of various types of heterogeneity areas in a space.

In order to assess semi-quantitatively the value of the relative level of structural heterogeneity of these polymer systems, their Porod invariants Q' were compared [21]:

$$Q' = \int_0^\infty q\,\tilde{I}(q)dq,$$

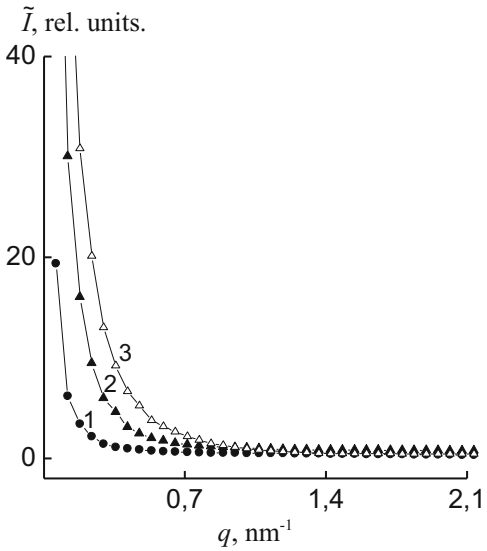

Fig. 3.3 Profiles of the intensity of small-angle X-ray scattering of (*1*) the IPEC pectin–P4VP, (*2*) the IMC pectin–Ag^+–P4VP, and the (*3*) IPEC–Ag nanocomposite

These values are invariant with respect to the shapes of the heterogeneity regions and are directly related to the rms values of electron density fluctuations ($<\Delta\rho^2>$) in a two-phase system:

$$Q' \propto < \Delta\rho^2 >,$$

Here, $<\Delta\rho^2> = \varphi_1\varphi_2(\rho_1-\rho_2)^2$, where φ_1 and φ_2 are the volume ratios of heterogeneity domains in a two-phase system and ρ_1 and ρ_2 are the electron densities of heterogeneity domains ($\varphi_1 + \varphi_2 = 1$) in a two-phase system. A comparison of the values of invariant Q' for the studied polymer systems (table) shows that the relative level of the structural heterogeneity increases significantly during the transition from the IPEC and the IMC into the nanocomposites based on the IPEC and Ag.

An evaluation of the effective sizes of the heterogeneity regions existing in these polymer systems was performed through the method from [19, 20] via calculation of structural parameters, such as the range of heterogeneity (range of inhomogeneity), l_p, which is directly related to the average diameters of heterogeneity regions, $<l_1>$ and $<l_2>$, in the two-phase system:

$$l_p = \varphi_2 < l_1 > = \varphi_1 < l_2 > .$$

After getting the result of the l_p calculation, the transition from the IPEC to the IMC was found to be accompanied with increasing of the effective size of region heterogeneity, while at transforming from the IMC into the IPEC–Ag nanocomposites, it decreased almost threefold (Table 3.1).

Table 3.1 Structural parameters and temperature transitions for the investigated polymer systems

Polymer system	l_p, nm	Q', rel. units	T_g, °C	T_f, °C	ε, % (T = 140 °C)
IPEC	35	10	63	207	23
IMC	43	24	57	199	18
IPEC–Ag	15	39	65	212	10

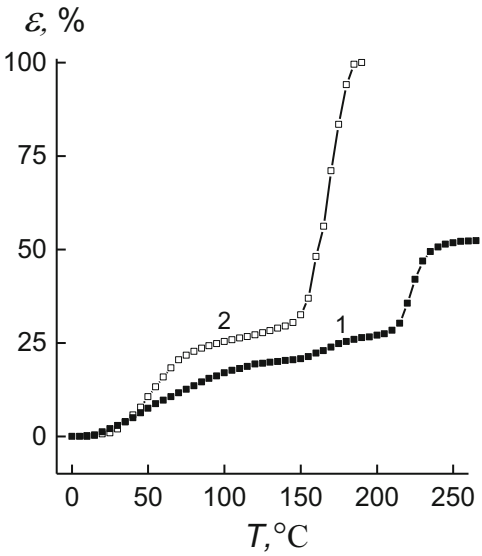

Fig. 3.4 Thermomechanical curves of (*1*) pectin and (*2*) P4VP. ε is relative value of penetration

Alongside with the structural organization of the IPEC, the IMC, and the nanocomposites based on IPEC–Ag, their thermomechanical behavior was studied.

Analysis of the pectin thermomechanical curve (see Fig. 3.4, curve *1*) demonstrated that temperature transitions which are associated with the glass transition and melting of the pectin crystallites occur in the temperature ranges 20–110 °C and 155–230 °C, respectively. Also, the strong deformational change has been observed in the melting process of pectin's crystalline phase [22]. As a contrast to anionic PE, the P4VP's thermomechanical curve has the usual (typical) shape with glass transition interval between 25 and 80 °C and flow temperature from 150 to 180 °C (curve *2*).

So, the shape of thermomechanical curve for IPEC (pectin–P4VP formed of equimolar quantities of anionic and cationic PE) is similar to P4VP's one with glass transition temperature in the range between 30 and 85 °C and flow point from 180 to 240 °C (Fig. 3.5, curve *1*).

Transferring from IPEC (pectin–P4VP) to the IMC (pectin–Ag^+–P4VP), on the latter curve a temperature shift at T = 200 °C appears, due to the $AgNO_3$ melting in the bulk of IPEC (curve *2*).

It is possible to conclude that in the temperature range 160–200 °C, the following processes take place: destruction of interpolyelectrolyte–metal complexes, transfer

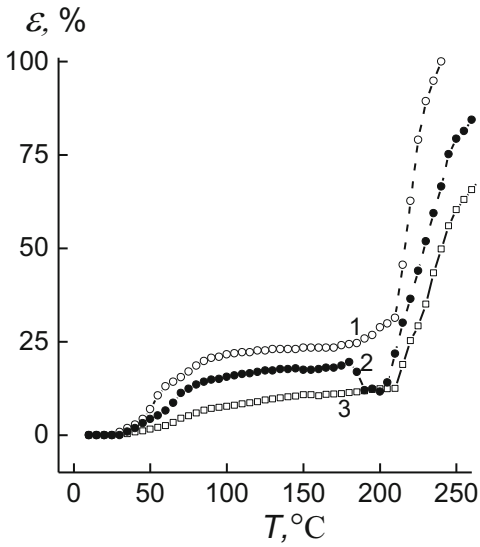

Fig. 3.5 Thermomechanical curves of (*1*) the IPEC pectin–P4VP, (*2*) the IMC pectin–Ag^+–P4VP, and (*3*) the IPEC–Ag nanocomposite

of $AgNO_3$ salt from ionic state to the crystalline one, and finally, its melting. So, changes occurred on the way from IPEC to IMC and to IPEC–Ag nanocomposite demonstrate that the level of relative penetration in these systems tends to be decreasing (Fig. 3.5).

Basing on the data of polymeric objects depicted in Fig. 3.5, the average-interval temperature values of glass transition, fluidity temperature, and relative penetration (in the high-elasticity state at $T = 140$ °C) have been determined (Table 3.1).

3.3 Structure and Antimicrobial Properties of Nanocomposites Based on Pectin–PEI and Ag Nanoparticles, Prepared by the Chemical and Thermal Reduction of Silver Ions in the Interpolyelectrolyte–Metal Complexes

To obtain the IPEC, pectin–polyethyleneimine; the IMC, pectin–Ag^+–polyethyleneimine; and nanocomposites of IPEC–Ag, the following reagents were used: anionic polyelectrolyte citrus pectin (Cargill Deutschland GmbH, Germany) with $M = 3 \times 10^4$, cationic polyelectrolyte anhydrous branched polyethyleneimine (PEI) (Aldrich) with $M_n = 1 \times 10^4$ and $M_w = 2.5 \times 10^4$, silver (I) nitrate ($AgNO_3$) (Aldrich) with $M = 169.9$, and sodium borohydride($NaBH_4$) (Aldrich) with $M = 37.83$.

IPEC samples were formed via mixing of 5% aqueous solutions of pectin and PEI taken at a molar ratio of 1:1, at $T = 20 \pm 2$ °C. IPEC as films were prepared via

pouring onto PTFE plates and drying up to constant masses at the same temperature. Dry IPEC films were washed in distilled water up to neutrality and dried repeatedly at 20 °C up to constant masses. The resulting films were 100 μm thick.

IMC samples were prepared via immersion of IPEC films into an aqueous solution of $AgNO_3$ with a concentration of 0.1 mol/L at $T = 20 \pm 2$ °C for 24 h. The colorless IPEC films became dark red. The absorption capacities of IMC films $A = 5.0$ mmol/g.

The chemical reduction of Ag^+ ions in the IMCs was conducted with $NaBH_4$ (a molar ratio of $[BH_4^-]$:$[Ag^+] \geq 1.0$) in an alkaline medium (pH 10.8) in a solvent mixture of water–isopropanol (4:1 vol %) at $T = 20 \pm 2$ °C for 3 h (until the release of gaseous bubbles ceased). The concentration of $NaBH_4$ in the aqueous alcohol solution was 0.1 mol/L.

Thermal reduction of Ag^+ ions in the IMC's volume was performed by heating of films to 100–160 °C within 30 min. Specimens were heated in the oven using precise thermal regulator VRT-3. Temperature regulation precision was ±0.5 °C.

As a result of the reduction, IMC films changed color from red to metallic.

The features of the structuring of the IPEC (pectin–PEI), the IMC (pectin–Ag^+–PEI), and nanocomposites of IPEC–Ag were studied by wide-angle X-ray diffraction on a DRON-4-07 diffractometer, whose X-ray optical scheme was used to "pass" primary-beam radiation through samples. X-ray diffraction studies were performed at $T = 20 \pm 2$ °C in CuK_α radiation monochromated with a Ni filter.

The antimicrobial activity of IPEC–Ag nanocomposites, prepared by chemical and thermal reduction of Ag^+ ions in IMC, was investigated using reference strains of opportunistic bacteria *Staphylococcus aureus* ATCC 6538 and *Escherichia coli* ATCC 35218 (as model gram-positive and gram-negative bacteria).

Investigations were carried out by agar diffusion method on a solid LB (Luria-Bertani) nutrient medium [23]. The nanocomposite films (size 10 × 10 mm) were placed on the surface of nutrient agar, which had been previously inoculated with 10 μL of bacterial suspension of *S. aureus* and *E. coli* at the rate of 2×10^5 CFU/ml. The plates were incubated at 37 °C for 24 h.

Clear zones, which has no bacteria around the film of composite, containing Ag were the indicator of antimicrobial activity. All experiments were repeated three times. The IPEC film was applied as a control sample.

The analysis of wide-angle X-ray diffractograms has shown that IPEC formed of pectin and PEI is characterized by short-range ordering during translation of fragments of oppositely charged polyelectrolyte macromolecular chains in space. This circumstance is indicated by the appearance of one diffuse diffraction maximum with $2\theta_m \sim 20.8°$ on the X-ray diffractogram of the IPEC sample (see Fig. 3.6, curve *1*). The average value of the period of short-range ordering of fragments of complementary macromolecular chains of oppositely charged polyelectrolytes in the IPEC (the Bragg distance between the macromolecule chains of anionic and cationic polyelectrolytes in the IPEC) is 4.3 Å, i.e., slightly less than that in the cationic polyelectrolyte.

However, the sorption of $AgNO_3$ by the IPEC sample and formation of the IPEC–Ag^+ IMC is accompanied by a change in the diffractogram. This result is proved by

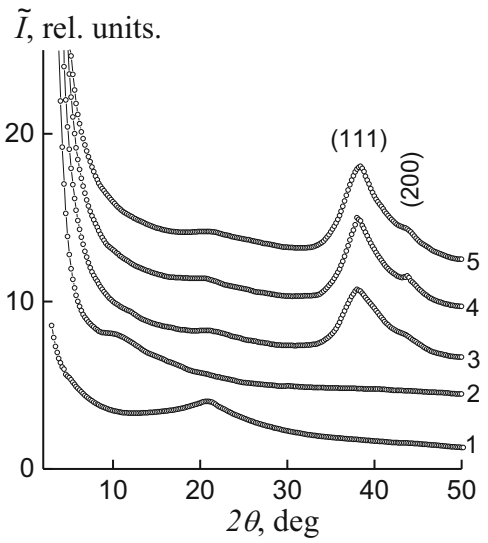

Fig. 3.6 Wide-angle X-ray diffractograms of (*1*) the IPEC, (*2*) the IMC, and (*3–5*) the IPEC–Ag nanocomposites obtained via the chemical reduction of Ag^+ ions in the IMC at molar ratios of BH_4^-:Ag^+ = (*3*) 1.0, (*4*) 2.0, and (*5*) 3.0

the appearance of an intense diffuse diffraction maximum at $2\theta_m \sim 11.2°$, featuring the structure polyelectrolyte–metal complex pectin–Ag^+–PEI [18] (curve *2*). In its turn, the amorphous halo disappears at $2\theta_m \sim 20.8°$, relating to the structural peculiarity of pectin–PEI IPEC. This indicates the full transfer of polyelectrolyte complexes into polyelectrolyte–metal complexes.

After the chemical reduction of the Ag^+ ions in the IMC with the use of sodium borohydride (a molar ratio of $[BH_4^-]$:$[Ag^+] = 1.0$) a nanocomposite based on the IPEC and Ag was formed. In the diffractogram of IPEC–Ag nanocomposite (curve *3*), the diffraction maximum at $2\theta_m \sim 11.2°$, which is typical of the abovementioned polyelectrolyte–metal complexes, is absent, unlike the two intense maxima at $2\theta_m = 38.2°$ and 43.8, corresponding to the crystallographic plan of the face-centered cubic lattice of silver with (111) and (200) indexes, respectively, and confirming presence of metal silver in the polymeric system.

With an increase in the amount of the reducing agent (a molar ratio of $[BH_4^-]$:$[Ag^+] = 2.0$), the X-ray diffractograms of nanocomposites based on the IPEC and Ag (curves *4*) show a significant increase in the intensity of the diffraction peaks at $2\theta_m = 38.2°$ and 43.8°, characterizing the structure Ag nanoparticles. The increase in the amount of the reducing agent (a molar ratio of $[BH_4^-]$:$[Ag^+] = 3.0$) does not change the structuring of the nanocomposites based on the IPEC and Ag nanoparticles (curves *4*, *5*).

Thus, according to wide-angle X-ray diffraction, it may be concluded that the molar ratio $[BH_4^-]$:$[Ag^+] = 2.0$ is optimum for the formation of IPEC–Ag nanocomposites.

Analysis of diffractograms of silver-containing nanocomposites prepared by thermal reduction of Ag^+ ions in IMC in the wide range of temperatures (100–160 °C) has shown, while the gradual increase of the temperature to $T = 150$ °C is

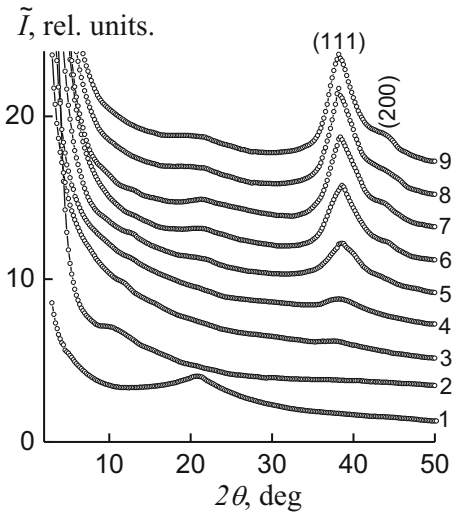

Fig. 3.7 Wide-angle X-ray diffractograms of (*1*) the IPEC, (*2*) the IMC, and (*3–9*) the nanocomposites obtained by the thermal reduction method from IMC at the temperatures (*3*) 100, (*4*) 110, (*5*) 120, (*6*) 130, (*7*) 140, (*8*) 150, and (*9*) 160 °C for 30 min

taking place, that the content of silver nanoparticles is growing up. So, the enhancing of intensity of two diffraction maxima at $2\theta_m \sim 38.2^o$ and 43.8^o confirms the presence of metal silver in the system (Fig. 3.7, curves *3–8*). The further increase in temperature (up to 160 °C) did not lead to the rise in the intensity of the diffraction maxima characterizing silver structure (Fig. 3.7, curves *8–9*).

At the further increase in temperature in IMC (up to $T = 160$ °C), the intensity of the diffraction maxima, characterizing the metal silver structure, did not change (Fig. 3.7, curves *8–9*).

Therefore, according to the WAXS data, we can conclude that the optimal temperature for Ag^+ ions' reduction in IMC with further formation of nanocomposite is to be 150 °C. In its turn, thermal reduction of silver ions is found out to take place owing to polyethyleneimine (namely, on account of electron transfer from the amino groups' nitrogen atoms of polyethyleneimine to Ag^+ ions) [1].

IPEC–Ag nanocomposites created by thermal reduction of Ag^+ ions in IMC at $T = 150$ °C within 30 min (Fig. 3.8) are found out to demonstrate higher antimicrobial activity against *S. aureus* and *E. coli* strains compared to IPEC–Ag, synthesized by chemical reduction (the chemical reduction of Ag^+ ions in the IMC was conducted with $NaBH_4$ (a molar ratio of $[BH_4^-]$:$[Ag^+] = 2.0$)). After incubation proceeds for 24 h at 37 °C, one can observe a clear zone around the films' contours, thus confirming inhibition of bacteria growth.

The growth inhibition's zone diameter for *S. aureus* was 27.6 mm for specimens prepared by thermal reduction and 18.2 mm for those obtained by chemical reduction. For *E. coli* these values are 26.6 mm and 17.6 mm, correspondingly (Table 3.2).

Active growth of the test bacteria and absence of growth inhibition have been observed in the test specimens (polymer film without nanoparticles).

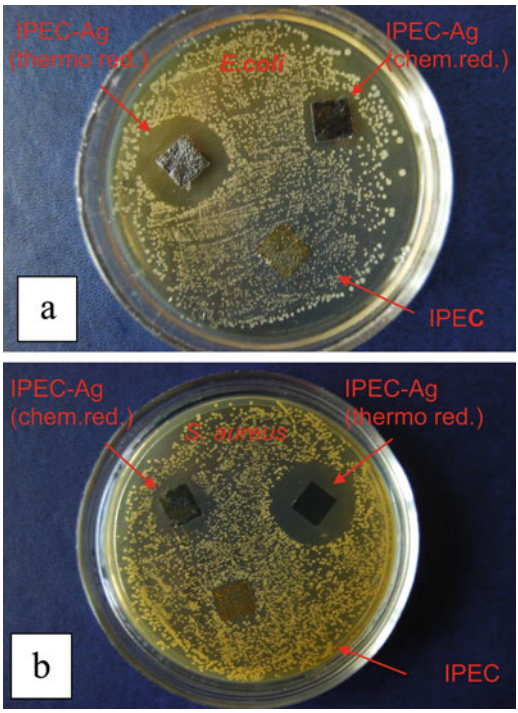

Fig. 3.8 Images of antimicrobial test results of agar plates containing IPEC–Ag nanocomposites, obtained via the thermoreduction and chemical reduction of Ag^+ ions in the IMC against *E. coli* (**a**) and *S. aureus* (**b**)

Table 3.2 Antimicrobial activity of the IPEC–Ag nanocomposites, prepared via the thermoreduction and chemical reduction of Ag^+ ions in the IMC

The method of obtaining nanocomposite films	Diameter of inhibition zone, mm	
	Staphylococcus aureus	*Escherichia coli*
Thermoreduction	IPEC–Ag 27.6 ± 1.2	IPEC–Ag 26.6 ± 1.2
Chemical reduction	IPEC–Ag 18.2 ± 0.8	IPEC–Ag 17.6 ± 0.6
Control sample	IPEC 0	IPEC 0

References

1. Demchenko V, Riabov S, Rybalchenko N, Goncharenko L, Kobylinskyi S, Shtompel V (2017) X-ray study of structural formation, thermomechanical and antimicrobial properties of copper-containing polymer nanocomposites obtained by the thermal reduction method. Eur Polym J 96:326–336
2. Demchenko V, Shtompel V, Riabov S (2016) Nanocomposites based on interpolyelectrolyte complex and Cu/Cu_2O core–shell nanoparticles: structure, thermomechanical and electric properties. Eur Polym J 75:310–316
3. Demchenko VL, Shtompel VI, Riabov SV (2015) DC field effect on the structuring and thermomechanical and electric properties of nanocomposites formed from pectin–Cu^{2+}–polyethyleneimine ternary polyelectrolyte–metal complexes. Polym Sci A 57:635–643

4. Demchenko VL, Shtompel VI (2014) Structuring, morphology, and thermomechanical properties of nanocomposites formed from ternary polyelectrolyte–metal complexes based on pectin, polyethyleneimine, and $CuSO_4$. Polym Sci B 56:927–934
5. Pomogailo AD, Kestelman VN (2005) Metallopolymer nanocomposites. Springer, New York
6. Rosi NL, Mirkin CA (2005) Nanostructures in biodiagnostics. Chem Rev 105:1547–1562
7. Ballauff M, Lu Y (2007) "Smart" nanoparticles: preparation, characterization and applications. Polymer 48:1815–1823
8. Ruiz P, Macanas J, Munoz M, Muraviev DN (2011) Intermatrix synthesis: easy technique permitting preparation of polymer-stabilized nanoparticles with desired composition and structure. Nanoscale Res Lett 6:343–348
9. Bruening ML, Dotzauer DM, Jain P, Ouyang L, Baker GL (2008) Creation of functional membranes using polyelectrolyte multilayers and polymer brushes. Langmuir 24:7663–7673
10. Deng Z, Zhu H, Peng B, Chen H, Sun YF, Gang XD, Jin PJ, Wang JL (2012) Synthesis of PS/Ag nanocomposite spheres with catalytic and antibacterial activities. ACS Appl Mater Interfaces 4:5625–5632
11. Prozorova GF, Pozdnyakov AS, Kuznetsova NP, Korzhova SA, Emel'yanov AI, Ermakova TG, Fadeeva TV, Sosedova LM (2014) Green synthesis of water-soluble nontoxic polymeric nanocomposites containing silver nanoparticles. Int J Nanomedicine 9:1883–1889
12. Barud HS, Regiani T, Marques RFC, Lustri WR, Messaddeq Y, Ribeiro SJL (2011) Antimicrobial bacterial cellulose-silver nanoparticles composite membranes. J Nanomater 2001:1–8
13. Shtompel VI, Sasa BS, Riabov SV, Kercha YY, Titov GV (2010) Polyelectrolyte complexes based on Na-carboxymethylcellulose and polyethyleneimine chloride: identification and structure. Polym J 32:204–209 (in Ukrainian)
14. Demchenko V, Shtompel V, Riabov S, Lysenkov E (2015) Constant electric and magnetic fields effect on the structuring and thermomechanical and thermophysical properties of nanocomposites formed from pectin–Cu^{2+}–polyethyleneimine interpolyelectrolyte – metal complexes. Nanoscale Res Lett 10:479–485
15. Kratky O, Pilz I, Schmitz PJ (1966) Absolute intensity measurement of small-angle x-ray scattering by means of a standard sample. J Colloid Interface Sci 21:24–34
16. Shtompel VI, Kercha YY (2008) Structure of linear polyurethanes. Naukova dumka, Kiev [in Russian]
17. Guinier A (2000) X-ray diffraction: in crystals, imperfect crystals, and amorphous bodies. Dower Publications, New York
18. Demchenko V, Riabov S, Shtompel V (2017) X-ray study of structural formation and thermomechanical properties of silver-containing polymer nanocomposites. Nanoscale Res Lett 12:235–240
19. Ruland W (1971) Small-angle scattering of two-phase systems: determination and significance of systematic deviations from Porod's law. J Appl Crystallogr 4:70–73
20. Perret R, Ruland W (1971) Eine verbesserte Auswertungsmethode fur die Rontgenkleinewinkelstreuung von Hochpolymeren. Kolloid Z Z Polym 247:835–843
21. Porod G (1982) In: Glatter O, Kratky O (eds) Small-angle X-ray scattering. Academic Press, London
22. Teitelbaum BJ (1979) Thermomechanical analysis of polymers. Nauka, Moscow [in Russian]
23. Case CL, Johnson TR (1984) Laboratory experiments in microbiology. Benjamin Cummings Pub Inc., Menlo Park